Structural Engineering and Mechanics, *Vol. 67, No. 6 (2018) 629-641*
DOI: https://doi.org/10.12989/sem.2018.67.6.629

A branch-switching procedure for analysing instability of steel structures subjected to fire

Andrea Morbioli[1a], Nicola Tondini[*1] and Jean-Marc Battini[2b]

[1]*Department of Civil, Environmental and Mechanical Engineering, University of Trento, Via Mesiano 77, 38123, Trento, Italy*
[2]*Department of Civil and Architectural Engineering, KTH, Royal Institute of Technology, Brinellvägen 23, 10044 Stockholm, Sweden*

(Received December 23, 2017, Revised July 5, 2018, Accepted July 7, 2018)

Abstract. The paper describes the development of a two-dimensional (2D) co-rotational nonlinear beam finite element that includes advanced path-following capabilities for detecting bifurcation instability in elasto-plasticity of steel elements subjected to fire without introducing imperfections. The advantage is twofold: i) no need to assume the magnitude of the imperfections and consequent reduction of the model complexity; ii) the presence of possible critical points is checked at each converged time step based on the actual load and stiffness distribution in the structure that is affected by the temperature field in the elements. In this way, the buckling modes at elevated temperature, that may be different from the ones at ambient temperature, can be properly taken into account. Moreover, an improved displacement predictor for estimating the displacement field allowed significant reduction of the computational cost. A co-rotational framework was exploited for describing the beam kinematic. In order to highlight the potential practical implications of the developed finite element, a parametric analysis was performed to investigate how the beam element compares both with the EN1993-1-2 buckling curve and with experimental tests on axially compressed steel members. Validation against experimental data and numerical outcomes obtained with commercial software is thoroughly described.

Keywords: branch-switching procedure; path-following technique; instability analysis; flexural buckling; co-rotational formulation; steel structures; fire; geometrical imperfections

1. Introduction

Numerical modelling by means of the finite element (FE) method has become very popular in the structural engineering community. This is also true when FE simulations are employed to analyse the structural fire behaviour. In this case, the structure undergoes loss of strength and stiffness as well as possible load redistribution owing to thermal action. In this respect, the fire design of steel structures takes particularly advantage of an accurate FE structural modelling that can considerably increase their economical convenience by reproducing beneficial mechanisms that can be established during the fire such as: catenary action of restrained beams (Liu *et al.* 2002, Yin and Wang 2002), membrane action of steel-concrete composite slabs (Bailey 2004, Li *et al.* 2007). Many researchers have therefore contributed to develop numerical models able to predict the behaviour of structures subjected to fire. For instance, in recent years the Fire Engineering group in Nanyang Technological University developed the tool FEMFAN (Tan *et al.* 2002); while Lien *et al.* (2010) proposed a Vector Form Intrinsic Finite Element (VFIFE) for the nonlinear study of steel structures under the effect of high temperatures. Along this line, two specifically-conceived FE software for the analysis of structures subjected to elevated temperature are SAFIR (Franssen and Gernay 2017) and VULCAN (Najjar and Burgess 1996, Bailey 2008). In addition, multipurpose software such as ABAQUS (2014), ANSYS (2016), DIANA (2016) have widen their library of thermomechanical elements to expand the treatment of these problems in the engineering practice. Thus, it is clear that the FE elements selected to model structures under fire action need to capture highly nonlinear phenomena if the results can be considered representative of the actual behaviour. Therefore, the first part of the paper focuses on the main features of the proposed beam element that incorporates path-following capabilities.

It is well known that steel structures are sensitive to buckling phenomena (Dimopulos and Gantes 2012, Sabuncu *et al.* 2016, Taleb *et al.* 2015). In particular, members subjected to compressive stresses, like columns, generally exhibit bifurcation buckling. Moreover, imperfections, both mechanical and geometrical, influence the behaviour of compression steel members. On these premises, buckling curves for design purposes were obtained and included in the Eurocodes (EN1993-1-1 2005, EN1993-1-2 2005). In this context, commercial FE codes commonly need to explicitly model these imperfections, though sometimes approximated via equivalent horizontal forces, in order to capture instability of an axially compressed element. For example, if for a single element

∗Corresponding author, Assistant Professor
E-mail: nicola.tondini@unitn.it
[a]Ph.D.
E-mail: morbioli.andrea@alice.it
[b]Professor
E-mail: jean-marc.battini@byv.kth.se

http://www.techno-press.com/journals/sem&subpage=7
ISSN: 1225-4568 (Print), 1598-6217 (Online)

the introduction of geometrical imperfections with sinusoidal shape and amplitude in the order of $h/1000$ (Franssen 2000), where h is the column length, is not particularly problematic; it is surely less straightforward when we have to deal with structural systems composed of several members. In fact, the buckling modes may not be easy to identify; thus, a linear elastic buckling analysis may be required a priori and FE codes used in structural fire engineering typically do not have this capability yet, e.g., SAFIR. In addition, the geometry of the FE model becomes more complicated to implement if the geometrical imperfections are explicitly accounted for and the choice of their magnitude represents another issue. In case of a fire, the buckling modes may change over time owing to degradation of material properties and the consequent variation of the relative stiffness between adjacent members. Load redistribution can also occur. Thus, if imperfections are introduced to force instability based on the buckling modes at ambient temperature, this choice may not even be good when the structure is affected by non-uniform thermal action. On these premises, this work aims to overcome the aforementioned issues by developing a 2D beam finite element that implements a branch-switching procedure able to capture at each converged solution possible elasto-plastic flexural instability at high temperature without introducing initial geometrical imperfections.

One classical alternative to perform branch-switching is to use the mode injection method (Wriggers and Simo 1990, Wagner and Wriggers 1988). This method can be used in both elastic (Zhou *et al.* 2015) and elasto-plastic (Battini, 2001) problems. However, in fire analysis, this approach is not suitable since it is very difficult to determine the amplitude of the buckling mode that will be used as predictor and it is not sure that the procedure will converge on the secondary path. In fact, there is a lack of works regarding the development of such techniques for applications in structural fire engineering. Thus, the paper is mainly devoted to close this gap and intends to highlight the practical implications by comparing the results both with the EN1993-1-2 buckling curve (2005) and with experimental tests on axially compressed steel elements as well as with case studies representative of steel-framed structures subjected to fire.

In the design practice, low computational demand is sought and beam FEs are typically employed to model columns and beams unless local instabilities are foreseen. In addition, nonlinear analyses require iterative procedures to converge to an equilibrated solution. Thus, in a nonlinear FE formulation a good choice of the displacement predictor can entail faster convergence. In this respect, the paper presents an optimization of standard convergence procedure, based on an improved displacement predictor at the beginning of each time step.

The article is articulated as follows: Section 2 describes the co-rotational framework and the local shallow arch Bernoulli formulation; Section 3 provides insight into the integration of the constitutive material law at high temperature; Section 4 describes the improved displacement predictor and presents the development of the branch-switching procedure; Section 5 shows the numerical examples aimed at validating the conceived beam finite element against experimental and simulated data with ABAQUS and SAFIR; Section 6 describes the branch-switching capabilities on numerical examples and the practical implications; Section 7 draws the conclusions and future perspectives.

2. Co-rotatıonal formulatıon

The idea of the co-rotational method is to decompose the motion of the element into rigid body and deformational part. During the rigid body motion, a local coordinate system, fixed to the element, moves and rotates with it. The deformational part is measured in this local system. The internal force vector and tangent stiffness matrix are first calculated with reference to the local system and then transformed with regard to the global one by using the transformation matrices relating local and global nodal quantities. The main advantage of the method is that with an appropriate choice of the element length, the local deformations are small. Consequently, existing linear elements or elements with a low order of nonlinearity can be used as local formulations.

2.1 Co-rotational framework

The co-rotational basic formulation for a two-dimensional beam element is hereinafter presented. The description follows what introduced in Crisfield (1991) and subsequently reported in Battini (2001). Since the co-rotational theory is based on the use of two different reference systems, it is essential to define a relation between the local and global expressions of the internal force vector and tangent stiffness matrix. Fig. 1 shows the kinematics quantities that are involved in the element motion according to the co-rotational formulation.

As shown in Fig. 1 the co-rotational beam is represented by a two-node element whose node 1 and 2 coordinates referred to the global fixed reference system (x_{glob}, y_{glob}) are respectively (x_1, y_1) and (x_2, y_2). A second moving local reference system (x_{loc}, y_{loc}) is then introduced. Different vectors for global $\mathbf{q_{glob}}$ and local displacement $\mathbf{q_{loc}}$ are respectively defined

$$\mathbf{q_{glob}} = \begin{bmatrix} u_1 & v_1 & \theta_1 & u_2 & v_2 & \theta_2 \end{bmatrix}^T \tag{1}$$

$$\mathbf{q_{loc}} = \begin{bmatrix} \bar{u} & \bar{\theta}_1 & \bar{\theta}_2 \end{bmatrix}^T \tag{2}$$

The components of $\mathbf{q_{loc}}$ are obtained according to

$$\bar{u} = l_n - l_0 \tag{3}$$

$$\bar{\theta}_1 = \theta_1 - \alpha \tag{4}$$

$$\bar{\theta}_2 = \theta_2 - \alpha \tag{5}$$

Where l_o and l_n represent the initial and the current

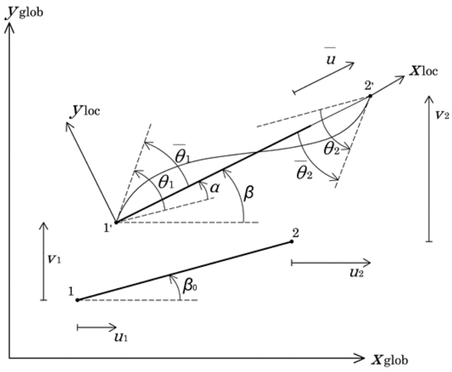

Fig. 1 2D co-rotational formulation

length of the element, respectively, while α is the rigid angle of rotation. All the new quantities can be then computed as

$$l_o = \left[\left(x_2 - x_1 \right)^2 + \left(y_2 - y_1 \right)^2 \right]^{1/2} \tag{6}$$

$$l_n = \left[\left(x_2 + u_2 - x_1 - u_1 \right)^2 + \left(y_2 + v_2 - y_1 - v_1 \right)^2 \right]^{1/2} \tag{7}$$

$$\sin\alpha = c_0 s - s_0 c \tag{8}$$

$$\cos\alpha = c_0 c + s_0 s \tag{9}$$

with

$$c_0 = \cos\beta_0 = \frac{1}{l_0}\left(x_2 - x_1 \right) \tag{10}$$

$$c = \cos\beta = \frac{1}{l_n}\left(x_2 + u_2 - x_1 - u_1 \right) \tag{11}$$

$$s_0 = \sin\beta_0 = \frac{1}{l_0}\left(y_2 - y_1 \right) \tag{12}$$

$$s = \sin\beta = \frac{1}{l_n}\left(y_2 + v_2 - y_1 - v_1 \right) \tag{13}$$

The correlation between virtual local and global displacements is reported in Eq. (14).

$$\boldsymbol{\delta}\mathbf{q}_{\mathbf{loc}} = \mathbf{B}\,\boldsymbol{\delta}\mathbf{q}_{\mathbf{glob}} \tag{14}$$

in which the transformation matrix **B** is function of the element current length l_n and angle β

$$\mathbf{B} = \begin{bmatrix} -c & -s & 0 & c & s & 0 \\ -s/l_n & c/l_n & 1 & s/l_n & -c/l_n & 0 \\ -s/l_n & c/l_n & 0 & s/l_n & -c/l_n & 1 \end{bmatrix} \tag{15}$$

After having introduced the relation between the local and the global virtual displacements through the definition of the transformation **B** matrix, it is then possible to obtain the correlation between the local value of the internal forces $\mathbf{f_{loc}}$ and local tangent stiffness matrix $\mathbf{K_{loc}}$ and the corresponding global quantities, $\mathbf{f_{glob}}$ and $\mathbf{K_{glob}}$. By exploiting the virtual work principle in both local and global reference systems and by using Eq. (14), the relation between $\mathbf{f_{loc}}$ and $\mathbf{f_{glob}}$ leads

$$\mathbf{f_{glob}} = \mathbf{B^T}\,\mathbf{f_{loc}} \tag{16}$$

where the internal local forces that define $\mathbf{f_{loc}}$ are

$$\mathbf{f_{loc}} = \left[N \quad M_1 \quad M_2 \right]^T \tag{17}$$

Subsequently, the relation between global and local expression of the tangent stiffness matrix $\mathbf{K_{glob}}$ and $\mathbf{K_{loc}}$ is derived by differentiating Eq. (16) and it yields

$$\mathbf{K_{glob}} = \mathbf{B^T}\,\mathbf{K_{loc}}\,\mathbf{B} + \frac{\mathbf{z}\,\mathbf{z^T}}{l_n} N + \frac{1}{l_n^2}\left(\mathbf{r}\,\mathbf{z^T} + \mathbf{z}\,\mathbf{r^T} \right) \cdot \left(M_1 + M_2 \right) \tag{18}$$

in which **r** and **z** terms Eqs. (19)-(20) are respectively

$$\mathbf{r} = \left[-c \quad -s \quad 0 \quad c \quad s \quad 0 \right]^T \tag{19}$$

$$\mathbf{z} = \left[s \quad -c \quad 0 \quad -s \quad c \quad 0 \right]^T \tag{20}$$

The local force vector $\mathbf{f_{loc}}$ and local tangent stiffness matrix $\mathbf{K_{loc}}$ depend on the specific definition introduced for the local formulation.

2.2 Local formulation

In the previous section the relation between local and global quantities of the force vector and the tangent stiffness matrix were derived. The following step consists in the definition of the local quantities based on the specific choice of the local formulation. As previously mentioned, one of the main advantages of the co-rotational approach is the possibility to adopt different formulations of the local deformations. In this way, it is possible to derive finite elements with different characteristics. Although a linear local Bernoulli as well as a Timoshenko formulation were implemented, for brevity only a local shallow arch Bernoulli beam theory that includes a low-order nonlinearity in the strain field is thoroughly reported.

2.2.1 Local shallow arch Bernoulli (LSAB) element

The local shallow arch formulation employs the classical assumptions of the local linear Bernoulli element but with a different definition of the local strain. This element uses an average measure for the axial strain in order to avoid membrane locking, but with a nonlinear definition of the local strain.

$$\varepsilon = \frac{1}{L}\int_L \left[\frac{\partial u}{\partial x} + \frac{1}{2}\left(\frac{\partial v}{\partial x} \right)^2 \right] \mathrm{d}x - \frac{\partial^2 v}{\partial x^2} y = \frac{\bar{u}}{L} + \frac{1}{15}\bar{\theta}_1^2 - \frac{1}{30}\bar{\theta}_1\bar{\theta}_2 + \\ + \frac{1}{15}\bar{\theta}_2^2 + y\left[\left(\frac{4}{L} - 6\frac{x}{L^2} \right)\bar{\theta}_1 + \left(\frac{2}{L} - 6\frac{x}{L^2} \right)\bar{\theta}_2 \right] \tag{21}$$

Now, by differentiating the strain

$$\delta\varepsilon = \frac{\delta\bar{u}}{L} + \frac{2}{15}\bar{\theta}_1\delta\bar{\theta}_1 - \frac{1}{30}\bar{\theta}_1\delta\bar{\theta}_2 - \frac{1}{30}\bar{\theta}_2\delta\bar{\theta}_1 + \frac{2}{15}\bar{\theta}_2\delta\bar{\theta}_2 + + y\left[\left(\frac{4}{L} - 6\frac{x}{L^2}\right)\delta\bar{\theta}_1 + \left(\frac{2}{L} - 6\frac{x}{L^2}\right)\delta\bar{\theta}_2\right] = \mathbf{A}\,\boldsymbol{\delta}\mathbf{q}_{\mathbf{loc}} \tag{22}$$

By using the virtual work theorem, $\boldsymbol{\delta}\mathbf{q}_{\mathbf{loc}}^{\mathbf{T}}\,\mathbf{f}_{\mathbf{loc}} = \int_V \delta\varepsilon^T \sigma\,\mathrm{d}V$, it is obtained

$$\mathbf{f}_{\mathbf{loc}} = \int_V \mathbf{A}^{\mathbf{T}}\,\sigma\,\mathrm{d}V \tag{23}$$

The local tangent stiffness matrix is computed by differentiation of Eq. (23)

$$\boldsymbol{\delta}\mathbf{f}_{\mathbf{loc}} = \int_V \mathbf{A}^{\mathbf{T}}\,\delta\sigma\,\mathrm{d}V + \int_V \delta\left(\mathbf{A}^{\mathbf{T}}\,\sigma\right)\mathrm{d}V \tag{24}$$

By taking into account that $\delta\sigma = E_n\,\delta\varepsilon$, where E_n is the tangent modulus that is derived by the integration of the material constitutive law, the previous equation can be reformulated as

$$\boldsymbol{\delta}\mathbf{f}_{\mathbf{loc}} = \int_V \mathbf{A}^{\mathbf{T}}\,E_n\,\mathbf{A}\,\boldsymbol{\delta}\mathbf{q}_{\mathbf{loc}}\,\mathrm{d}V + \int_V \mathbf{L}\,\sigma\,\boldsymbol{\delta}\mathbf{q}_{\mathbf{loc}}\,\mathrm{d}V \tag{25}$$

and the local tangent matrix reads

$$\mathbf{K}_{\mathbf{loc}} = \int_V \mathbf{A}^{\mathbf{T}}\,E_n\,\mathbf{A}\,\mathrm{d}V + \int_V \mathbf{L}\,\sigma\,\mathrm{d}V \tag{26}$$

with

$$\mathbf{L} = \begin{bmatrix} 0 & 0 & 0 \\ 0 & 2/15 & -1/30 \\ 0 & -1/30 & 2/15 \end{bmatrix} \tag{27}$$

2.2.2 Constitutive material laws

The local shallow arch Bernoulli formulation relies on uniaxial constitutive material laws. Typical stress-strain relationships assumed in the design of steel structures are: elastic-perfectly plastic behaviour, elasto-plastic behaviour with isotropic or kinematic hardening. In this respect, the integration of the material constitutive law to obtain the local force vector and the tangent stiffness matrix is performed by means of the classical numerical integration according to Gauss quadrature. For a uniaxial constitutive material law no iterations are needed at the Gauss point level and the element was developed to allow the user to select from two up to five Gauss integration points along the element length and up to fifteen points at the cross-sectional level. This allows taking into account the plasticity diffusion with a different order of precision. In Section 3, the effect of the temperature on the integration of the material constitutive laws is described in depth.

3. Behaviour of steel at high temperature

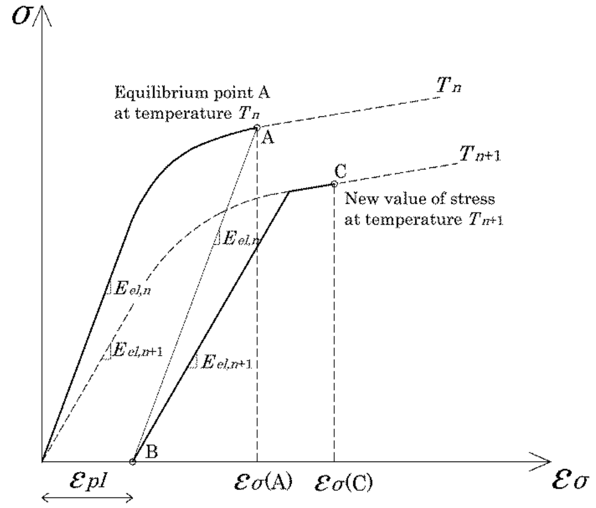

Fig. 2 Integration of material uniaxial constitutive law at high temperature

In the previous paragraph, the co-rotational beam formulation was introduced. Under this form, the finite element is potentially able to perform nonlinear analysis by taking into account geometrical and material nonlinearity at ambient temperature. The purpose is now to extend the field of application of the finite element by introducing the effects of temperature for the numerical analysis of steel structures subjected to fire.

3.1 Integration of the steel constitutive law at high temperature

With reference to the uniaxial material constitutive law that describes the behaviour of steel at high temperature, the total strain can be decomposed in

$$\varepsilon_{tot}\left(\sigma,T,t\right) = \varepsilon_{\sigma}\left(\sigma,T\right) + \varepsilon_{th}\left(T\right) \tag{28}$$

Where in Eq. (28) ε_{tot} represents the total strain that is obtained as the sum of the stress-related strain ε_σ and the thermal strain ε_{th}. In general, a term that describes explicitly the creep strain ε_{cr} can be also added. However, we considered that the effect of the creep strain was implicitly included in the stress-strain relation as for EN1993-1-2 (2005).

After defining the strain quantities, it is then possible to specify the integration scheme that allows to compute at each new step and for each Gauss integration point the updated value of stress and tangent modulus that allow to derive the new expression of the local internal force vector and the local tangent stiffness matrix. The procedure depends on the specific adopted local formulation. In case of the local shallow arch Bernoulli element the integration of constitutive law was performed on a uniaxial law, as depicted in Fig. 2. The proposed model is based on the assumption of isotropic hardening. Under the effect of temperature the axial strain increment is given by

$$\Delta\varepsilon = \Delta\varepsilon_\sigma + \Delta\varepsilon_{th} \tag{29}$$

Where $\Delta\varepsilon_\sigma$ is the strain increment induced by stress while $\Delta\varepsilon_{th}$ is the thermal strain increment that can be expressed as

$$\Delta\varepsilon_{th} = \alpha_{th}\Delta T = \alpha_{th}\left(T_{n+1} - T_n\right) \tag{30}$$

In Eq. (30), α_{th} represents the thermal expansion coefficient, T_n and T_{n+1} the temperature at step n and n+1, respectively.

With reference again to Fig. 2, when a thermal increment ΔT is introduced from a converged solution at temperature T_n point (A), the updating procedure that allows to compute the new values of stress and tangent modulus $E_n=d\sigma/d\varepsilon$ at temperature T_{n+1} follows the curve A-B-C. The A-B curve represents the unloading until point B with residual strain ε_{pl}, that is assumed as a reference point in order to process a new loading at temperature T_{n+1} (B-C curve), this choice is set due to the assumption that the plastic strain is not affected by a temperature variation (Franssen 1990). A similar procedure is also reported in Lie *et al.* (2010). Point C represents the updated value of stress that is obtained at temperature T_{n+1}.

4. Path following procedures

The computational analysis of nonlinear structures requires the solution of large systems of nonlinear algebraic equations in order to compute the equilibrium path of the system. At each step, the equilibrium equations are solved by using Newton-Raphson iterations preceded by a predictor (Cardona and Huespe 1999). In this context, the purpose of this section is to address two specific issues. The first one is related to the choice of an efficient predictor. The second one is related to the computation of post-buckling paths on the perfect structure, i.e., without introducing imperfections. For that, specific procedures have to be introduced in order to first detect the bifurcation point and then to perform the branch-switching to the secondary path. In commercial FE software this problem is overcome by introducing small geometrical imperfections or alternatively small loads at some specific points. However, with such a method, the instability phenomena cannot be exactly described and the choice of the shape and the amplitude of the imperfections is not always an easy task.

4.1 Displacement predictor

In this section, an improved displacement predictor is described to increase the efficiency of the structural nonlinear analysis. In fact, in a displacement-based FE code a good displacement predictor can dramatically reduce the number of iterations to achieve convergence. In classical nonlinear static analysis the predictor is usually chosen by assuming that the structure behaves linearly during the step. Consequently, the predictor is calculated by considering that the increments of the nodal displacements and the applied forces are related by the tangent stiffness matrix at the equilibrium point. However, this approach is not possible in fire analysis since the applied forces are constant.

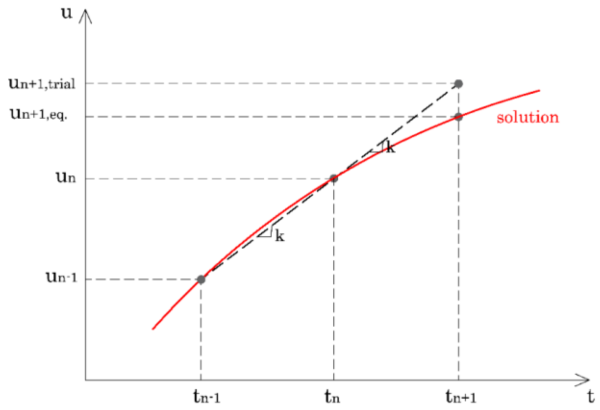

Fig. 3 Scheme of the proposed displacement predictor

For this reason, a classical predictor used in fire analysis (called here as Predictor 1) starts the iterative process with the solution (displacement vector) computed at the last converged equilibrium point, i.e.,

$$\mathbf{u_{n+1}} = \mathbf{u_n} \tag{31}$$

This predictor is very simple but obviously not optimal since it is clear that the change of temperature during the step will indeed give additional displacements. For this reason, a second predictor (Predictor 2) is here proposed in order to get a more realistic value of the trial displacement solution. This predictor is calculated by assuming a linear variation of the displacement vector between the steps n-1, n and n+1, as shown in Eq. (32) and Fig. 3

$$\mathbf{u_{n+1}} = \mathbf{u_n} + \frac{t_{n+1} - t_n}{t_n - t_{n-1}}\left(\mathbf{u_n} - \mathbf{u_{n-1}}\right) \tag{32}$$

where not only the last converged solution $\mathbf{u_n}$ but also the second last equilibrium point $\mathbf{u_{n-1}}$ is exploited to provide a more realistic value of the trial displacement solution $\mathbf{u_{n+1}}$.

The efficiency of the two predictors was numerically tested on two different case studies as reported in Section 5.3.

4.2 Branch-switching procedure

The procedure that has been implemented to study instability problems of steel compressed members is herein described. This methodology is capable of detecting the presence of critical points along the fundamental equilibrium path and to perform a branch-switching to the secondary path without defining initial geometrical imperfections. This procedure was presented for elastoplastic instability problem in Battini and Pacoste (2002) and is now widen to study the instability of compressed structural elements exposed to fire. The idea of the method, initially introduced by Petryk (1992), is that along a stable deformation path, the displacements $\mathbf{u}$ corresponds to an absolute minimum of the functional J defined by

Table 1 Analyzed case studies

	Case study	Analysed problem
1	Simple supported beam	-Test on displacement predictor -Evaluation of high geometrical nonlinearity -Comparison with ABAQUS (2014)
2	L frame	-Introduction of EN1993-1-2 constitutive law for carbon steel at high temperature -Test on displacement predictor -Comparison with SAFIR (Franssen 2005)
3	EHR frame	-Validation against experimental data (Rubert and Schaumann 1986)

$$J = \frac{1}{2}\mathbf{u}^{\mathbf{T}}\mathbf{K}\mathbf{u} - \mathbf{u}^{\mathbf{T}}\mathbf{f}_{\mathbf{ex}} \tag{33}$$

Where $\mathbf{K}$ is the global stiffness matrix and $\mathbf{f}_{\mathbf{ex}}$ the vector of the external loads. The critical point is detected by computing the lowest eigenvalues of $\mathbf{K}$ calculated at each converged solution. If one or more negative eigenvalues are present in the diagonal matrix, then it means that the equilibrium point is unstable and that a bifurcation point has been passed. Classical one side bisections can be introduced in order to identify the exact position of the critical point by simply reducing the step size.

Once the critical point is obtained, the first equilibrium point on the secondary path is computed by minimizing J. In order to ensure that the minimisation procedure does not end on the fundamental path, a new predictor $\mathbf{u}_{\mathbf{n+1,BS}}$ is constructed by adding a small perturbation vector to the predictor presented in Eq. (32). In principle, any random perturbation vector can be taken. However, since an eigenvalue analysis has been already performed to determine the bifurcation point, it is judicious to take the eigenvector $\mathbf{v}$ associated to the lowest negative eigenvalue of $\mathbf{K}$. This gives

$$\mathbf{u}_{\mathbf{n+1,BS}} = \mathbf{u}_{\mathbf{n}} + \mathbf{\Delta} + \frac{\|\mathbf{\Delta}\|}{100}\frac{\mathbf{v}}{\|\mathbf{v}\|} \tag{34}$$

with

$$\mathbf{\Delta} = \frac{t_{n+1} - t_n}{t_n - t_{n-1}}(\mathbf{u}_{\mathbf{n}} - \mathbf{u}_{\mathbf{n-1}}) \tag{35}$$

The minimization procedure consists in solving at each iteration the nonlinear system

$$\left(\mathbf{K}^{\mathbf{i}} + \mu\mathbf{I}\right)\mathbf{\Delta u} = -\mathbf{r}^{\mathbf{i}} \tag{36}$$

where $\mathbf{I}$ is the identity matrix, $\mathbf{r}$ is the residual vector while μ is a coefficient that as proposed in Fletcher (1987) can be set equal to either 1.1 λ_{min}, where λ_{min} is the lowest eigenvalue of $\mathbf{K}$, or to 0 if $\mathbf{K}$ is positive definite. At the end of each iteration the displacement is updated by means of

$$\mathbf{u}^{\mathbf{i+1}} = \mathbf{u}^{\mathbf{i}} + \mathbf{\Delta u} \tag{37}$$

The successive equilibrium points on the secondary path are then computed by using Predictor 2 Eq. (32) and classical Newton-Raphson iterations.

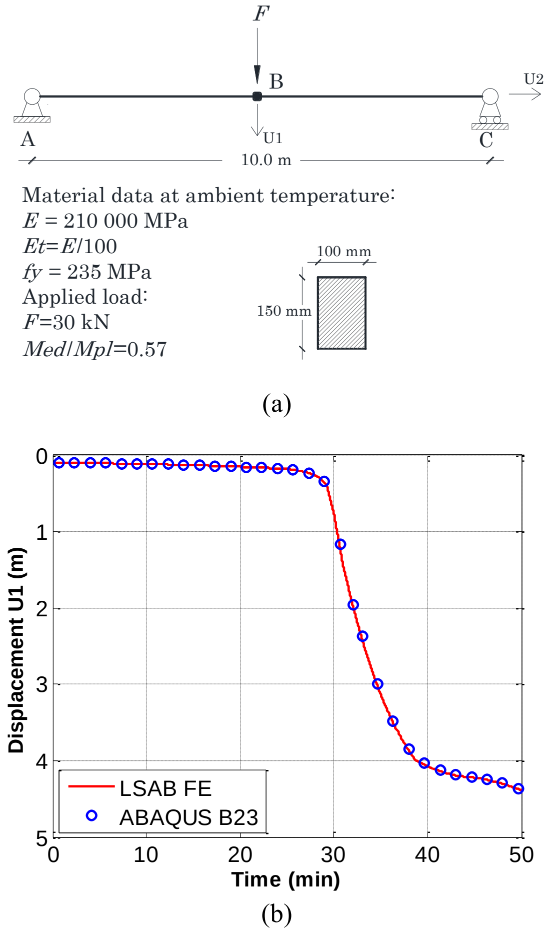

Fig. 4 Case study 1: (a) geometry and data; (b) comparison of vertical displacement U1 at midspan

5. Validation of the beam FE

Different meaningful case studies were used to validate the proposed beam FE, as reported in Table 1. Case studies 1 and 2 were exploited to assess the capabilities of the beam FE to capture highly nonlinear problems in steel members caused by thermal exposure. Moreover, in order to investigate the potential practical implications of the element, comparison with experimental data (Rubert and Schaumann 1986) is described in Case study 3. In all analyses, the maximum strain was limited to 15%, which corresponds to moderate strain.

5.1 Case study 1: Simply supported beam

The first case study is representative of a simply supported beam with a concentrated load at midspan. The geometry, applied load, cross section and material properties at ambient temperature are reported in Fig. 4(a). The ratio between the applied bending moment M_{ed} at midspan and the plastic moment M_{pl} of the cross section is 0.57.

The thermal action on the beam is represented by the ISO 834 standard heating curve. Since the element is not able to perform heat transfer analysis, the cross-section temperature distribution, that is assumed to be uniform in

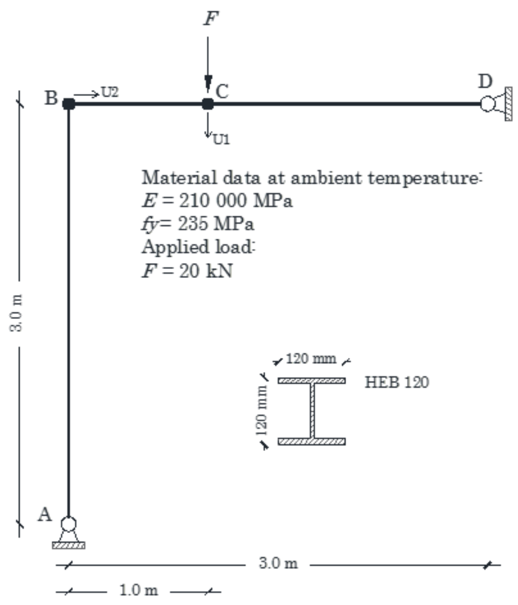

(a)

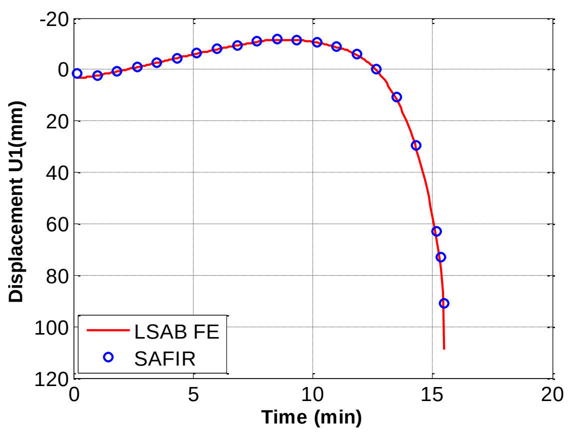

(b)

Fig. 5 Case study 2: (a) geometry and data; (b) comparison of the vertical displacement U1 at C

the beam, was computed according to the mass lumped concept provided in EN1993-1-2 (2005) by considering the section exposed on all sides. The structure was also studied, under the same assumptions, by means of the commercial software ABAQUS (2014) using the Bernoulli B23 thermomechanical beam element. In this way, it was possible to meaningfully compare the local shallow arch Bernoulli (LSAB) formulation implemented in the developed FE.

A bilinear material constitutive law with yield strength f_y = 235 MPa and hardening tangent modulus equal to E_t=E/100 was used to represent the steel material constitutive law. The degradation of the steel mechanical properties at elevated temperature followed the recommendations given in EN1993-1-2 (2005). A constant thermal expansion coefficient α_{th}=1.2 10^{-5}°C^{-1} was used. Fig. 4(b) illustrates the evolution in time of the vertical displacement at midspan computed with the LSAB formulation. Twenty LSAB finite elements with two Gauss integration points along the beam length and fifteen in the cross-section height were used. The outcomes showed the ability of the developed finite element to treat problems characterised by high nonlinearities induced by thermal effects. In particular, the case study highlighted well the geometrical nonlinearity with the final midspan vertical displacement that is in the order of 50% of the initial beam span length. Moreover, good agreement with the predictions of ABAQUS multipurpose software is shown.

5.2 Case study 2: L frame

The aim of Case study 2 is to model a structural frame with steel material properties given in EN1993-1-2 (2005) and a realistic member cross-section profile. The model consists of a double hinged, L-shape steel frame whose structural members are made of HEB 120 profiles of S235 steel grade. The dimension of the frame and the data are reported in Fig. 5(a). A concentrated load force was applied to the beam midspan and was kept constant during the simulation whilst the temperature in the cross section of both the beam and the column varied in time based on the thermal exposure of the ISO 834 heating curve applied to all sides. The temperature distribution was assumed uniform in the cross section and computed again according to a mass lumped concept. The computer program SAFIR (Franssen and Gernay 2017) was used for the validation. It was specifically conceived for the numerical analysis of structures in fire. Its beam element is a fibre-based Bernoulli element. A fibre formulation was used because SAFIR is able to also solve the heat transfer problem in a sequential way. In order to have a consistent comparison, the same uniform temperature evolution was imposed to the SAFIR beam element cross-section that was composed of an adequate number of fibres. 60 LSAB FEs with fifteen Gauss integration points in the cross section and two integration points along the FE length were used to model the L-frame. The stress-strain relation of carbon steel at elevated temperature and the relative reduction factors of mechanical properties as well as the steel relative elongation provided by EN1993-1-2 (2005) were employed in the analysis. Fig. 5(b) shows the results of the analysis in terms of vertical displacement of point C. Very good agreement is exhibited between the two models that provided the same time of collapse.

5.3 Efficiency of the displacement predictor

The efficiency of the predictor presented in Section 4.1 was investigated on Case Study 1 and Case Study 2 that are characterised by a different level of nonlinearity. In both cases, the application of the improved predictor, i.e., Predictor 2, entailed a drastic reduction of the number of iterations that are necessary to achieve convergence.

The results of the simulations are reported in Tables 2 and 3. In Case Study 1, the effect of the geometrical nonlinearity was significant because the vertical deflection was approximately equal to ½ of the beam initial span. The use of Predictor 2 implies a reduction of the number of required iterations to achieve the new converged solution of

Table 2 Comparison of the efficiency of the two analysed displacement predictors as a function of the number of iterations required to achieve convergence (Case Study 1-Section 5.1)

No. finite elements	Total number of iterations inside Newton-Raphson corrector procedure		
	Predictor 1	Predictor 2	Reduction number of iterations (%)
6	10393	4043	61
8	10499	4600	56
10	10490	4532	57
100	10752	5260	51

Table 3 Comparison of the efficiency of the two analysed displacement predictors as a function of the number of iterations required to achieve convergence (Case Study 2-Section 5.2)

No. finite elements	Total number of iterations inside Newton-Raphson corrector procedure		
	Predictor 1	Predictor 2	Reduction number of iterations (%)
30	3229	1750	46
48	3235	1750	46
60	3247	1758	46

about 60%.

In Case Study 2, characterised by lower nonlinearity, the advantage obtained with Predictor 2 is once again significant, i.e., a reduction of about 46%. In sum, the displacement predictor based on the linear combination of the two previous converged solutions showed better performance in terms of computational cost.

5.4 Validation against experimental data: Case study 3: EHR frame

A comparison against experimental data is hereinafter described to show how the developed FE is able to predict the real behaviour of steel structures exposed to fire. In particular, the test conducted by Rubert and Schaumann (1986) on a frame under the combined action of mechanical and thermal loads was exploited. In greater detail, the experimental test, referred as EHR series, was an L frame composed of IPE80 profiles and exposed to the ISO 834 standard heating curve. The EN1993-1-2 temperature dependent stress-strain relationship (2005) was used to integrate the material properties whereas the degradation of the initial modulus of elasticity E, the proportional limit f_p and the yield point f_y were assumed in accordance with the authors' guidance (Rubert and Schaumann 1986). Forty LSAB finite elements with two Gauss integration points along the finite element length and fifteen in the cross-section height were employed. The results reported in Fig. 6(b) show reasonably good agreement with the experimental evidences. In particular, the critical temperature obtained through the numerical simulation was T_{num}=466°C and that observed experimentally T_{test}=475°C, which entails an error of less than 2%.

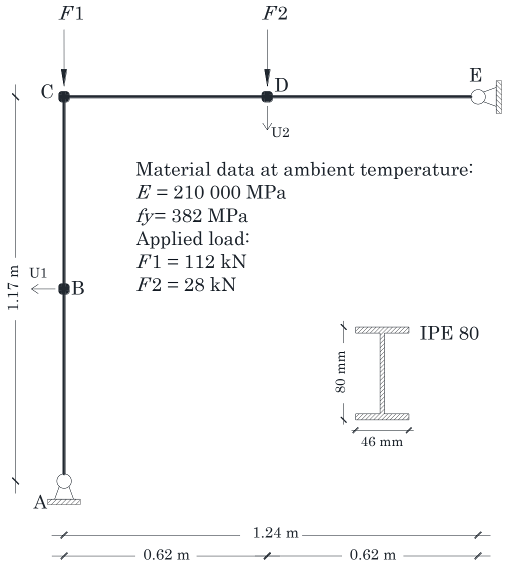

(a)

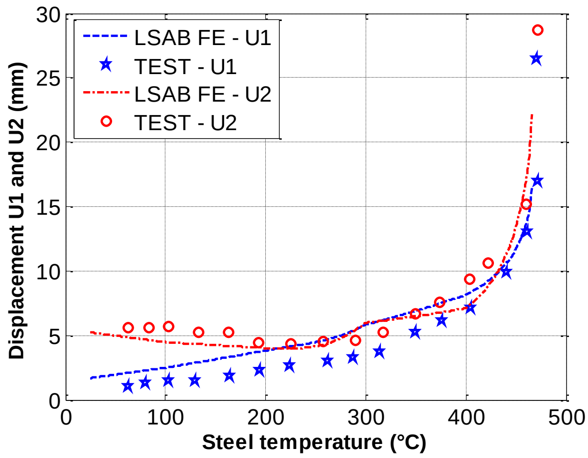

(b)

Fig. 6(a) geometry of the EHR frame (b) evolution of U1 and U2 displacements.

6. Instability analysis of steel structures exposed to fire

6.1 Case Study 1: Axially loaded column

The capabilities of the branch-switching procedure described in Section 4.2 to analyse instability problems of steel structures exposed to fire were initially proved by investigating a simple case study of flexural buckling of a compressed column whose geometry, cross section, slenderness λ and material properties of at ambient temperature are reported in Fig. 7(a). The simulation was performed with twenty LSAB finite elements, fifteen Gauss integration points in the cross section and two integration points along the finite element length. In order to check the accuracy of the analysis, a comparison with an equivalent ABAQUS model was made. The evolution in time of the steel temperature, which is uniform in the cross section, is reported in Fig. 7(b) and it is based on the standard heating

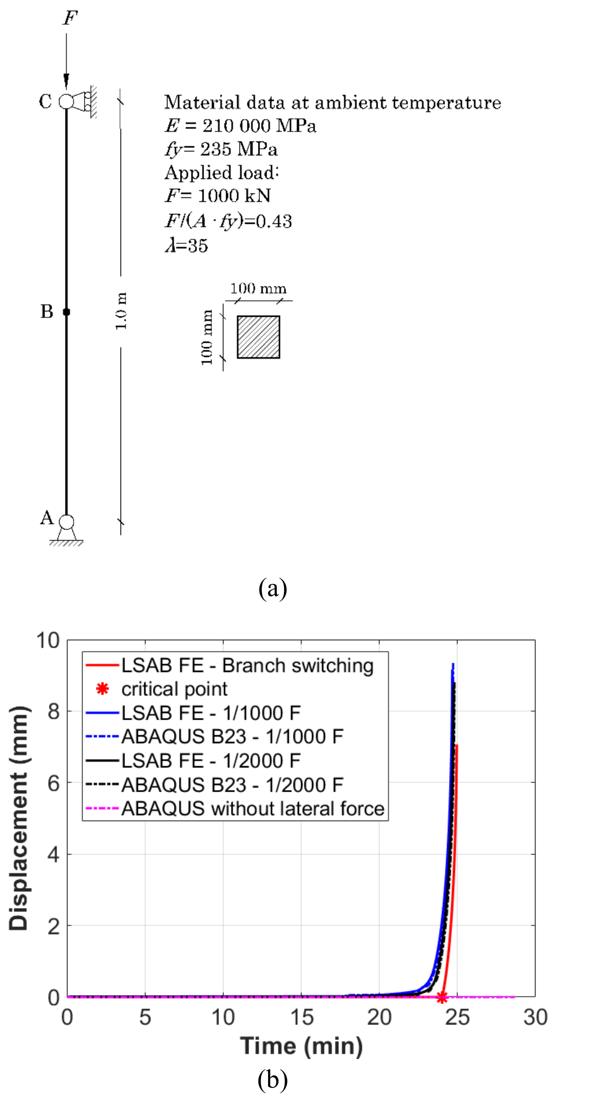

Fig. 7 Compressed column subjected to instability: (a) geometry (b) Compressed column: transverse displacement at node B

curve exposure. The steel stress-strain relation as well as the reduction factors of the mechanical properties were assumed according to the EN1993-1-2 (2005).

The analysis showed that the section exhibited first plastic strains at t = 17 min and 48 s that corresponded to a steel temperature of 397.4°C. At this step, the value of the proportional limit f_p is below 100 MPa, which is the applied compressive stress. Moreover, the value of the tangent modulus reduced progressively owing to the combined effect of strain and temperature increase. The critical point was identified at t = 24 min with steel temperature equal to 533.7°C. For this value of temperature, the tangent modulus E_n is 12180 MPa, which is very close to the theoretical buckling value computed according to the Euler critical load that reads

$$E_{cr} = \frac{Fl^2}{\pi^2 I} \cong 12159 \text{ MPa} \tag{38}$$

After this point, the new solution was obtained by using the minimization procedure described in Section 4.2 and the secondary equilibrium path was then followed. The results of the analysis are shown in Fig. 7(b), where the critical point of branch switching to the secondary equilibrium path is clearly identified. This suggests that the implementation of the branch-switching procedure to study the behaviour of structural elements subjected to elevated temperature has been successful. Then, the same case study was performed with the procedure that is commonly used in commercial finite element software, which consists in introducing an arbitrary lateral force or, alternatively, in modifying the geometry of the problem by means of an initial geometrical imperfection. As a result, a lateral force was introduced at the midspan node B and its initial value was chosen adequately small - 1/1000 F or 1/2000 F -. An analogous analysis with an equivalent ABAQUS model of the column composed of 20 B23 elements was also carried out. The comparison of the two procedures highlighted some advantages that are intrinsic of the implemented path-following technique. Firstly, the solution obtained with ABAQUS exhibited an initial transverse displacement for the effect of the lateral force necessary to force instability, which was not present in the ideal case where the perfect column was only subjected to the compression load. During the analysis, the transverse displacement increased for the combined effects of plasticity and of thermal action that progressively reduced the mechanical properties of steel. Conversely, by employing the branch-switching procedure the column exhibited only axial displacements until the critical point that marked bifurcation to the secondary equilibrium path. In Fig. 7 the ABAQUS solution without any imperfections and lateral forces is also highlighted and failure occurred due to crushing at a substantial increased time.

6.2 Case Study 2: Axially loaded portal frame

The second case study is based on a portal frame whose columns are loaded with identical vertical concentrated load. The frame is uniformly heated according to the ISO 834. The geometry, cross section and material properties at ambient temperature are reported in Fig. 8(a). The model was made of a fine mesh based on ninety LSAB FE, fifteen gauss integration points in the cross section and two integration points along the element length. With fifteen Gauss points the full cross-section plasticization could be captured. The comparison of results was performed by means of an equivalent ABAQUS model composed of B23 finite element that included horizontal forces of magnitude 1/500 F and 1/1000 F applied rightward at node B, respectively. In both models, the steel material properties are those given in EN1993-1-2 (2005).

The analysis showed that the critical bifurcation point was reached after 13 min and 54 s that corresponded to a value of steel temperature equal to 673.3°C. At this time step, a negative eigenvalue in the diagonal of the eigenvalue matrix related to the stiffness matrix of the structure obtained at the last equilibrium point was found. The branch-switching procedure then proceeded by introducing a perturbation vector that contained the eigenvector associated with the most negative eigenvalue of the stiffness

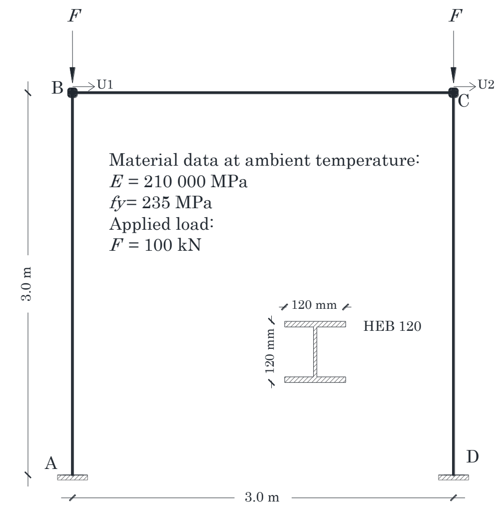

(a)

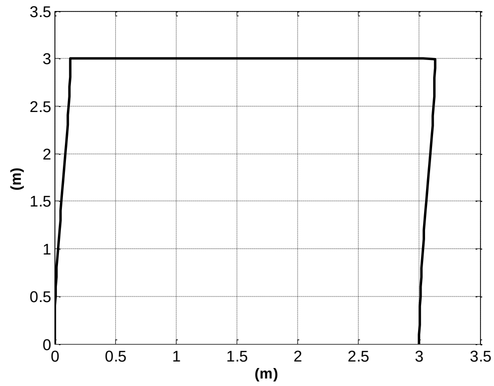

(b)

Fig. 8 Portal frame: (a) geometry; (b) eigenvector shape associated to the minimum eigenvalue registered at the critical point

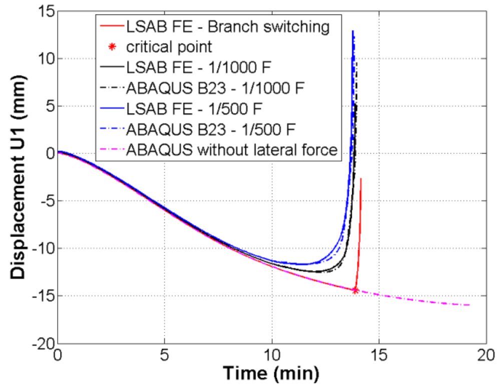

(a)

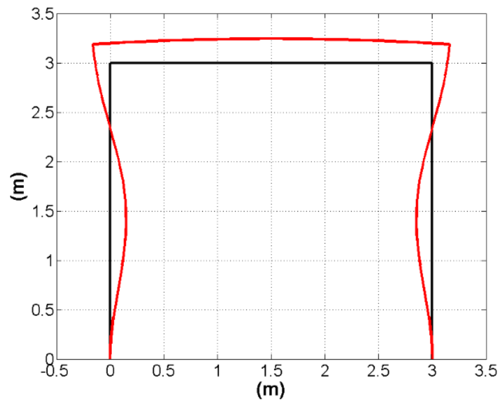

(b)

Fig. 9 Instability analysis of a heated portal frame: (a) evolution of the transverse displacement with time; (b) deformed shape at failure of the heated portal frame modelled in ABAQUS without imperfections and lateral forces (scale 10x)

matrix **K** whose shape typical of a sway mode is depicted in Fig. 8(b).

Unlike the case of the axially compressed column in which the displacement up to the critical point is limited to the axial component, here the effect of thermal dilatation also produced transverse displacement. The modified displacement predictor, based on branch switching, introduced a perturbation that successively produced the collapse of the structure due to sway instability. As a result, this procedure has the major advantage to detect possible bifurcation points of a structural system that is subjected to both mechanical and thermal loads. In Fig. 9 the results in terms of horizontal displacement time evolution are shown. It is possible to observe that the branch-switching procedure predicted the bifurcation point and the elasto-plastic instability failure without the need to explicitly model the initial imperfections. When horizontal forces were applied instability intervened with smoother transition as shown in Fig. 9(a). Conversely, in the ABAQUS model without neither imperfections nor lateral forces, the failure mode occurred 10 min later and with a symmetric failure mode that did not take into account the sway nature of the frame, as depicted in Fig. 9(b).

6.3 Case Study 3: 3-Storey steel frame

The third case study considers the simulation of a whole sway steel frame (Couto *et al.* 2013). The steel frame is a 3-storey 3-bay steel frame, as shown in Fig. 10(a). The steel grade is S235. The fire is represented by the ISO 834 heating curve applied to unprotected columns and beams of the ground floor. The accidental load combination yields

$$Q_{d.fire} = G_k + A_d + \sum \psi_{2.i} Q_{k.i} \tag{39}$$

Where G_k are characteristic dead loads, A_d the indirect actions owing to fire, $\psi_{2.i}$ the combination factor and Q_k the characteristic live loads. For instance in Italy, the value of $\psi_{2.i}$ relative to wind loading is zero (NTC 2018). Thus, the introduction of global imperfections is fundamental to capture sway mode instabilities, above all if the fire scenario entails a symmetric thermal exposure of the structural elements. In fact, by heating up the columns and the beams of the ground floor according to the ISO 834 standard curve neither ABAQUS nor SAFIR 2016 are able to detect a sway mechanism of the perfect frame (Fig. 10(c) and Fig. 10(d)) and the failure time is increased by about 30%-from 750 s to 960 s-with respect to the frame modelled

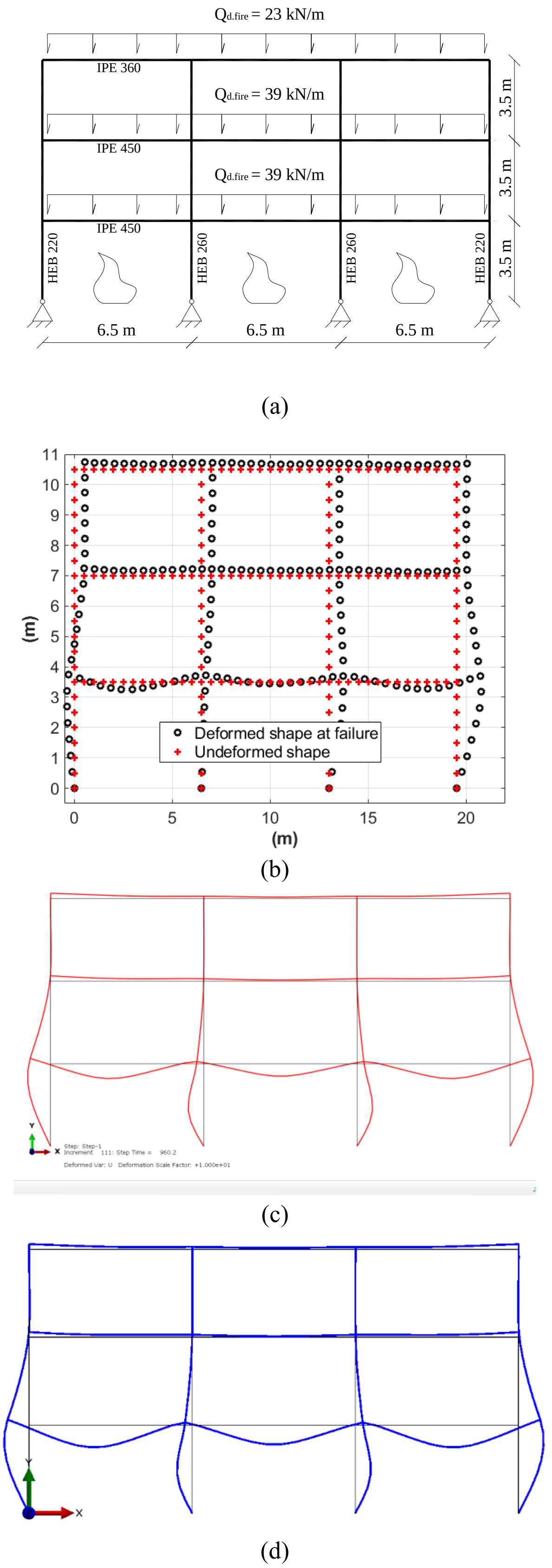

Fig. 10 3-storey steel frame: (a) Frame characteristics; (b) deformed shape at failure (t = 750 s) with branch switching (scale 10x); (c) deformed shape at failure (t = 960 s) ABAQUS (scale 10x); d) deformed shape at failure (t = 960 s) SAFIR 2016 (scale 10x)

with beam elements that include the proposed branch-switching procedure (Fig. 10(b)). According to EN1993-1-1 (2005), the imperfections shall be included according to buckling shapes in the most unfavourable direction and form. However, since the thermal loads typically vary with time also the buckling modes do, because of the thermal effect on the structure, e.g., thermal expansion, possible load redistribution, loss of stiffness etc. Thus, for a generic thermal exposure, e.g. natural fire, the buckling mode shapes at ambient temperature are different from those at elevated temperature and it may be difficult to foresee them a priori. A linear buckling analysis performed at ambient temperature to identify the initial imperfections to be introduced into the model could be even misleading. Thus, some trials may be possibly needed. In this respect, the proposed element represents a useful tool to overcome this issue. For instance, by applying imperfections by means of notional horizontal forces applied at each floor in the SAFIR 2016 model, the mode of failure coincides with the one depicted in Fig. 10(b) and also the failure time decreases to 735 s. Moreover, this procedure can also be beneficial to avoid the introduction of member imperfections to capture the post-buckling behaviour of an axially restrained column or of a bracing element.

6.4 Parametric analysis and comparison with the buckling curve of EN1993-1-2

In Section 6.1-6.3, it was shown that the implementation of the branch-switching procedure in the proposed FE was fulfilled for analysing instability of steel structural systems exposed to fire without including initial geometrical imperfections. In Section 5.4 it was shown that the developed FE is able to well reproduce experimental outcomes, here, further practical implications of the procedure will be emphasised. In fact, the advantage to avoid the explicit modelling of the geometrical imperfections is clear: no need to assume the shape and the amplitude of the imperfections that also implies a reduced model complexity. However, this benefit becomes fully effective if it can be applied in practice to simulate instability problems of real steel structural members. On these premises, the capabilities of the branch-switching procedure of predicting the flexural buckling curve provided in EN1993-1-2 (2005) relatively to the behaviour of Class 1 or 2 compression steel members in fire with respect to the strong axis are investigated. The EN1993-1-2 buckling curve accounts for geometrical ($h/1000$ where h is the member height) and mechanical imperfections (residual stresses) (Franssen *et al.* 1995) and it provides the reduction factor for flexural buckling in fire condition χ_{fi} as a function of the relative slenderness at high temperature λ_{fi}. Therefore, the idea is to reproduce the flexural buckling curve by means of a parametric analysis by employing the proposed beam FE applied to axially compressed steel members and to compare it both with the one provided in EN1993-1-2 and with experimental tests performed at Braunschweig and at Stuttgart on 19 H-profiles with respect to the strong axis (Franssen *et al.* 1996). As a result, a series of pinned-pinned H-profiles were selected and loaded with a constant axial compression load N equal to 20% of the plastic axial

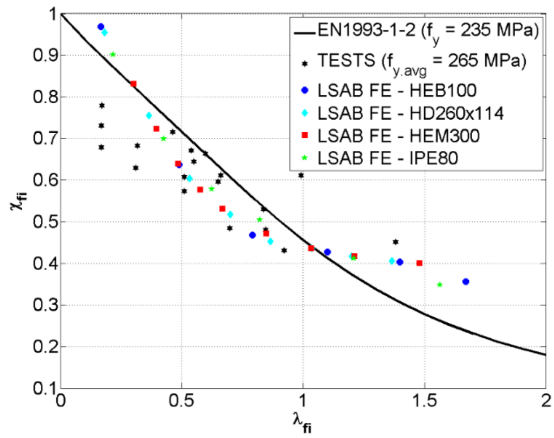

Fig. 11 Comparison between the buckling reduction factors obtained with the proposed FE and the buckling curve of EN1993-1-2 as well as test values

capacity of the cross section, i.e., to $N / A f_y = 0.20$, where A is the area of the cross section. The selected profiles were the following: HEB 100; HD 260×14; HEM 300 and IPE 80. The steel grade was S235 that implied a Class 1 cross-section classification in fire conditions (EN1993-1-2 2005). The EN1993-1-2 material properties of carbon steel (2005) were used. A uniform and linearly increasing temperature characterised by heating rate of 2.67°C/min was assigned to the cross section. Then, several analyses with varying relative slenderness at ambient temperature from 0.13 to 1.40 were carried out to cover a wide range of relative slenderness in fire condition. At the end of each analysis, which corresponded to member failure, the steel temperature T_{cr} was recorded and the flexural buckling reduction factor was computed according to Eq. (40)

$$\chi_{fi} = \frac{N}{k_{y.T} f_y A} \tag{40}$$

Where N is the applied load, $k_{y.T}$ is the reduction factor of yield strength at the critical temperature T_{cr}, f_y is the yield strength at ambient temperature and A is the cross-section area.

The comparison with the EN1993-1-2 buckling curve is shown in Fig. 11 and it suggests that the FE with branch-switching capabilities is conservative in predicting the buckling strength at elevated temperature of steel compressed H elements when the relative slenderness in fire condition is below 1.0. In fact, the average $\chi_{fi}(\lambda_{fi}< 1)$ is -7% with respect to the EN1993-1-2 buckling curve, whereas when $\lambda_{fi} \geq 1$, χ_{fi} is overestimated of about +20%. This difference is in line with what observed experimentally, i.e., $\chi_{fi}(\lambda_{fi} < 1)$=-12% and $\chi_{fi}(\lambda_{fi} \geq 1)$=+37% (although only two test values when $\lambda_{fi} \geq 1$) relative to EN1993-1-2 values computed with actual yield strength of the specimens. In conclusion, these promising results add value to the applicability domain of the proposed FE in the design practice that could rely on models without geometrical imperfections to simulate the buckling behaviour of steel structures at elevated temperature.

7. Conclusions

The paper described the development of a co-rotational two-dimensional beam element to study instability problems of steel structures exposed to fire by means of a branch-switching procedure. A local shallow arch Bernoulli formulation was implemented. Validation against experimental data and numerical simulations carried out with commercial software, such as ABAQUS and SAFIR, showed good agreement. The branch-switching procedure capable of analysing instability problems in elasto-plasticity of steel structures by detecting bifurcation points of secondary equilibrium paths without explicitly including initial geometrical imperfections was successfully implemented. This entails a benefit in terms of practical implications in the context of structural fire FE modelling. First, since there is no need to explicitly introduce the geometrical imperfections to detect critical points, the geometry of the structural model is less complex. In addition, no assumptions on the amplitude of the imperfections have to be made. Then, critical bifurcations points that depend on the actual distribution of mechanical loads and temperatures in the elements at each converged solution can be identified. This implies a major advantage for the analysis of steel structures in fire for which, in general, the buckling mode shapes vary with time and consequently any introduced imperfections based on buckling analysis at ambient temperature may not be representative of the actual behaviour at elevated temperature. Furthermore, comparison of the parametric analysis performed in this work on axially compressed steel H profiles with the EN1993-1-2 buckling curve showed conservative χ_{fi} values for λ_{fi}<1 (-7%) and overestimated χ_{fi} values for $\lambda_{fi} \geq 1$ (+20%). Nevertheless, this trend is consistent with experimental outcomes found in literature. This characteristic suggests that the beam FE has promising properties in predicting the buckling strength of real steel members in compression, which is an important added value for design applications. Finally, an improved displacement predictor based on the linear combination of the two previous converged solutions was proposed. It allowed faster convergence with a significant decrease in the number of iterations-up to about 60%-with respect to a displacement predictor based on the previous converged solution only. Future works will be addressed to extend this procedure to co-rotational 3D beam and shell elements with thermomechanical capabilities.

Acknowledgments

The financial support of the University of Trento as well as the scientific and logistic support of the KTH-Stockholm are gratefully acknowledged.

References

Bailey, C.G. (1998), "Development of computer software to simulate the structure behaviour of steel-framed buildings in fire", *Comput. Struct.*, **67**, 421-438.

Bailey, C.G. (2004), "Membrane action of slab/beam composite floor systems in fire", *Eng. Struct.*, **26**, 1691-1703.

Battini, J.M. (2001), "Co-rotational beam elements in instability problems", Ph.D. Dissertation, Department of Structural Engineering KTH, Stockholm, Sweden.

Battini, J.M. and Pacoste, C. (2002), "Plastic instability of beam structures using corotational elements", *Comput. Meth. Appl. Mech. Eng.*, **191**, 5811-5831.

Cardona, A. and Huespe, A. (1999), "Evaluation of simple bifurcation points and post-critical path in large finite rotation problems", *Comput. Meth. Appl. Mech. Eng.*, **175**, 137-156.

Couto, C., Vila Real, P., Lopes, N. and Rodrigues, J.P. (2013), "Buckling analysis of braced and unbraced steel frames exposed to fire", *Eng. Struct.*, **49**, 541-559.

Crisfield, M.A. (1991), *Non-Linear Finite Element Analysis of Solids and Structures*, Essentials, Wiley, Chichester, U.K.

Dimopoulos, C.A. and Gantes, C.J. (2012), "Comparison of alternative algorithms for buckling analysis of slender steel structures", *Struct. Eng. Mech.*, **44**(2), 219-238.

Fletcher, R. (1987), *Practical Methods of Optimization*, 2nd Edition, Wiley.

Franssen, J.M. (1990), "The unloading of building materials submitted to fire", *Fire Safety J.*, **16**(3), 213-227.

Franssen, J.M., Schleich, J.B. and Cajot, L.G. (1995), "A simple model for the fire resistance of axially-loaded members according to Eurocode 3", *J. Constr. Steel Res.*, **35**, 49-69.

Franssen, J.M., Schleich, J.B., Cajot, L.G. and Azpiazu, W. (1996), "A simple model for the fire resistance of axially-loaded members-comparison with experimental results", *J. Constr. Steel Res.*, **37**(3), 175-204.

Franssen, J.M. (1997), *Contributions à la Modélisation des Incendies et de leurs Effets sur les Batiments*, Faculté des Sciences Appliquées, Chercheur Qualifié du F.N.R.S, Université de Liège.

Franssen, J.M. (2000), "Failure temperature of a system comprising a restrained column submitted to fire", *Fire Safety J.*, **34**, 191-207.

Franssen, J.M. and Gernay, T. (2017), "Modeling structures in fire with SAFIR®: Theoretical background and capabilities", *J. Struct. Fire Eng.*, **8**(3), 300-323.

Li, G.Q., Guo, S.X. and Zhou, H.S. (2007), "Modeling of membrane action in floor slabs subjected to fire", *Eng. Struct.*, **29**, 880-887.

Lien, K.H., Chiou, Y.J., Wang, R.Z. and Hsiao, P.A. (2010), "Vector form intrinsic finite element analysis of nonlinear behavior of steel structures exposed to fire", *Eng. Struct.*, **32**, 80-92.

Liu, T.C.H., Fahad, M.K. and Davies, J.M. (2002), "Experimental investigation of behaviour of axially restrained steel beams in fire", *J. Constr. Steel Res.*, **58**, 1211-1230.

Najjar, S.R. and Burgess, I.W. (1996), "A nonlinear analysis for three-dimensional steel frames in fire conditions", *Eng. Struct.*, **18**, 77-89.

NTC (2018), *Norme Tecniche per le Costruzioni, Ministero delle Infrastrutture e dei Trasporti*, Rome, Italy

Petryk, H. and Thermann, K. (1992), "On discretized plasticity problems with bifurcation", *Int. J. Sol. Struct.*, **29**(6), 745-765.

Rubert, A. and Schaumann, P. (1986), "Structural steel and plane frame assemblies under fire actions", *Fire Safety J.*, **10**, 173-184.

Sabuncu, M., Ozturk, H. and Yashar, A. (2016), "Static and dynamic stability of cracked multi-storey steel frames", *Struct. Eng. Mech.*, **58**(1), 103-119.

Tan, K.H., Ting, S.K. and Huang, Z.F. (2002), "Visco-elasto-plastic analysis of steel frames in fire", *J. Struct. Eng.*, **128**(1), 105-114.

Taleb, C.E., Ammari, F. and Adman, R. (2015), "Analytical study of buckling profile web stability", *Struct. Eng. Mech.*, **53**(1), 147-158.

Wagner, W. and Wriggers, P. (1988), "Simple method for the calculation of postcritical branches", *Eng. Comput.*, **5**(2), 103-109.

Wriggers, P. and Simo, J.C. (1990), "A general procedure for the direct computation of turning and bifurcation points", *Int. J. Numer. Meth. Eng.*, **30**, 155-176.

Yin, Y.Z. and Wang, Y.C. (2004), "A numerical study of large deflection behaviour of restrained steel beams at elevated temperatures", *J. Constr. Steel Res.*, **60**, 1029-1047.

Zhou, Y., Stanciulescu, I., Eason, T. and Spottswood, M. (2015), "Nonlinear elastic buckling and postbuckling analysis of cylindrical panels", *Fin. Elem. Analy. Des.*, **96**, 41-50.

EN1993-1-1 (2005), *Eurocode 3 Design of Steel Structures-Part 1-1. General Rules and Rules for Buildings*, European Committee for Standardization, Brussels, Belgium.

EN1993-1-2 (2005), *Eurocode 3 Design of Steel Structures-Part 1-2. General Rules Structural Fire Design*, European Committee for Standardization, Brussels, Belgium.

ABAQUS Version 6.14 (2014), *Users' Manual*, Dassault Systèmes.

DIANA Version 10.1 (2016), *Users' Manual*, DIANA FEA BV.

ANSYS Version 17.0 (2016), *Users' Manual*, ANSYS, Inc.

PL